Journal of the Iranian Chemical Society (2023) 20:2713–2725
https://doi.org/10.1007/s13738-023-02868-w

ORIGINAL PAPER

Anti-carcinoma and anti -microbial behavioral studies for octahedral synthesized Schiff base metal complexes

Hanan Abd El-Halim[1] · Omnia Y. El-Sayed[2] · Gehad G. Mohamed[2,3]

Received: 2 May 2021 / Accepted: 2 December 2021 / Published online: 13 September 2023

Abstract

2,2′-((1Z-1′Z) (1,3-diphenylpropane-1,3-diylidene) bis (azanylylidene)) dibenzoic acid (H_2L) Schiff base ligand, derived from condensation reaction in a molar ratio 2:1 between anthranilic acid and dibenzoyl methane, respectively. Cr(III), Mn(II), Fe(III), Co(II), Ni(II), Cu(II), Zn(II) and Cd(II) complexes were obtained from 1:1 (ligand: metal salt) reaction. Elemental analyses, IR, ^{1}H NMR, UV–Vis, ESR, mass spectra, conductivity, and magnetic susceptibility measurements as well as thermal (TG/DTG) analyses have been used to conclude the molecular structure of the prepared complexes. From the analytical and spectroscopic tools, the stoichiometry of the complexes was found to be of ML type with octahedral geometry. The conductivity values supported the electrolytic nature of Cr(III) and Fe(III) complexes and non- electrolytic nature of the remaining complexes. From IR studies, the involvement of two azomethine nitrogen atoms and two carboxylate oxygen has been proved as tetradendate binding sites of the ligand. Screening Schiff base and its complexes for their antimicrobial activity against *Streptococcus pneumoniae* and *Bacillus subtilis as G + bacteria*; *Pseudomonas aeruginosa* and *Escherichia coli as G− bacteria*) and fungi (*Aspergillus fumigatus*; *Syncephalastrum racemosum*; *Geotricum candidum* and *Candida albicans*) has been conducted by disk diffusion method. The Comparison between the antimicrobial activity of the metal complexes and the free ligand showed the advancement of the metal complexes. Unfortunately, no promising anti-tumor activity has been detected for the ligand and its metal complexes as they were evaluated against human cancer (MCF-7 cells viability).

Keywords Schiff base complexes · Anthranilic acid · Dibenzoyl methane · Antimicrobial activity · Anticancer activity

Introduction

Schiff base ligands synthesized from the condensation reaction of an amino compound with carbonyl compounds are very essential ligands in modern coordination and medicinal chemistry. The Schiff base ligands and their metal complexes widely used for industrial purposes such as pigments, catalysts, intermediates in organic synthesis and as polymer stabilizers [1]. They also exhibit a broad range of biological activities such as antibacterial, antifungal, herbicidal, anti-inflammatory, anticancer, anti-diabetic, antileishmanial, antitumor and antipyretic properties [2–5].

The azomethine function group (–C=N–) of the Schiff base improve the formation of a stable complex. This linkage has special importance in elucidating the mechanism of transmination and racemization in biological system. The Schiff base complexes are used in the treatment of many diseases including cancer and as potential hypoxia-activated prodrugs [6]. The interest in preparation of new metal complexes gained the tendency of studying the interactions of metal complexes with DNA for their applications in biotechnology and medicine. Deoxyribonucleic acid (DNA) is the primary target molecule for most anticancer and antiviral therapies according to cell biologists. Investigation on the interaction of DNA with small molecules is important in the design of new type of pharmaceutical molecules. Schiff base constitutes an important class of nitrogen donor ligands and occupy a prominent position among the recent achievement in the field of coordination chemistry [6].

✉ Hanan Abd El-Halim
hanan.farouk@miuegypt.edu.eg;
hanan_farouk1@hotmail.com

[1] Pharmaceutical Chemistry Department, Faculty of Pharmacy, Misr International University, Cairo, Egypt

[2] Chemistry Department, Faculty of Science, Cairo University, Giza 12613, Egypt

[3] Nanoscience Department, Basic and Applied Sciences Institute, Egypt-Japan University of Science and Technology, New Borg El Arab, Alexandria 21934, Egypt

Cu(II), Ni(II) and Co(II) metal complexes which have bioinorganic relevance have been prepared with Schiff base ligand 2-furylglyoxal–anthranilic acid [7]. The results of antimicrobial activity studies of the complexes against some of the pathogenic bacteria and fungi confirm that metal complexes are much more active as compared to ligand fragments [7]. Novel Schiff bases have been reported by Kargar et al. [8–13]. The in vitro biological activities of the synthesized ligands and their copper(II) complexes were evaluated against *Staphylococcus aureus* and *Escherichia coli*. The activity data showed that the metal complexes have a promising biological potential comparable with the parent Schiff base ligands against bacterial species.

The aim of this work was to prepare eight novel metal complexes of Cr(III), Mn(II), Fe(III), Co(II), Ni(II), Cu(II), Zn(II) and Cd(II) from Schiff base ligand derived from a condensation reaction of anthranilic acid with dibenzoyl methane. Different physico-chemical techniques have been employed to characterize the prepared ligand and its metal complexes. Antimicrobial and anticancer activities of prepared compounds have been evaluated. The biological and antitumor activities revealed remarkable increase upon introducing the metal ions to the ligand center. Suggested molecular structures of the metal complexes have been performed.

Experimental

Materials and reagents

All chemicals used were of the analytical reagent grade (AR), and of highest purity available. Anthranilic acid, dibenzoyl methane, $CrCl_3.6H_2O$, $MnCl_2.2H_2O$, $FeCl_3.6H_2O$, $CoCl_2.6H_2O$, $NiCl_2.6H_2O$, $CuCl_2.2H_2O$, $ZnCl_2$ and $CdCl_2$ were provided from Acros, Sigma, Prolabo, Aldrich, BDH, Merck, and Strem Chemicals. Ethyl alcohol (90%), acetone and dimethylformamide (DMF) were used as organic solvents. Distilled water was usually used in all preparations.

Solutions

To prepare stock solutions of the Schiff base ligand and its metal complexes of 1×10^{-3} M, an accurately weighed amount of the complex was dissolved in dimethylformamide. Solutions have been used for measuring their UV–Vis spectra and molar conductivity.

Solution of anticancer study

Dimethylsulphoxide (DMSO) was used in cryopreservation of cells. RPMI-1640 medium (supplied in a powder form) was used for culturing and maintenance of the human tumor cell line and was. It was prepared by weighing 10.4 g medium which mixed with 2 g sodium bicarbonate, completed to 1 L with distilled water and shaked carefully till complete dissolution. The medium was then sterilized by filtration in a Millipore bacterial filter (0.22 lm). The prepared medium was kept in a refrigerator (4 °C) and checked at regular intervals for contamination. Before use, the medium was warmed at 37 °C in a water bath and supplemented with penicillin/streptomycin and Fetal Bovine Serum (FBS). 0.05% Isotonic Trypan blue solution was prepared in normal saline and was used for viability counting. 10% FBS (heat inactivated at 56 °C for 30 min), penicillin and streptomycin were used for the supplementation of RPMI-1640 medium prior to use. Trypsin was used for the harvesting of cells while, acetic acid was used for dissolving the unbound SRB dye. 0.4% Sulphorhodamine-B (SRB) dissolved in 1% acetic acid was used as a protein dye. 50 µl of trichloroacetic acid was added to 200 µl RPMI-1640 medium/well to yield a final concentration of 10% used for protein precipitation. 100% Isopropanol and 70% ethanol were used. Tris base 10 mM (pH 10.5) was used for SRB dye solubilization. 121.1 g of tris base was dissolved in 1000 ml of distilled water and pH was adjusted by HCl acid (2 M).

Instruments

The molar magnetic susceptibility was measured on powdered samples using the Faraday method. The diamagnetic corrections were made by Pascal's constant and $Hg[Co(SCN)_4]$ was used as a calibrant. Molar conductivities of 10^{-3} M solutions of the solid complexes in DMF were measured using Jenway 4010 conductivity meter. Mass spectra were recorded by the EI technique at 70 eV using MS-5988 GS-MS Hewlett–Packard instrument at the Microanalytical Center, National Center for Research, Egypt. The X-ray powder diffraction analyses were carried out using Philips Analytical X-ray BV, diffractometer type PW 1840. Radiation was provided by copper target (Cu anode2000 W) high intensity X-ray tube operated at 40 kV and 25 mA. Divergence and the receiving slits were 1 and 0.2, respectively. FT-IR spectra were recorded on a Perkin-Elmer 1650 spectrometer (4000–400 cm^{-1}) in KBr pellets. ^1H NMR spectra, as a solution in DMSO-d_6, were recorded on a 300 MHz Varian-Oxford Mercury at room temperature using TMS as an internal standard. Electron spin resonance spectra were also recorded on JES-FE2XG ESR spectrophotometer at Microanalytical Center, Tanta University. UV–Vis spectra were carried out on UV mini-1240, UV–Vis spectrophotometer, Shimadzu. Microanalyses of carbon, hydrogen and nitrogen were carried out at the Microanalytical Center, Cairo University, Egypt, using CHNS-932 (LECO) Vario Elemental Analyzer. Analyses of the metals followed the dissolution of the solid complexes in concentrated HNO_3, neutralizing the diluted aqueous solutions with ammonia

and titrating the metal solutions with EDTA. The thermogravimetric analyses (TG and DTG) of the solid complexes were carried out from room temperature to 1000 °C using a Shimadzu TG-50H thermal analyzer. The anticancer activity was performed at the National Cancer Institute, Cancer Biology Department, Pharmacology Department, Cairo University. The optical density (O.D.) of each well was measured spectrophotometrically at 564 nm with an ELIZA microplate reader (Meter tech. R 960, USA). The antimicrobial activities were carried out at the Microanalytical Center, Cairo University, Egypt.

Synthesis of Schiff base ligand

The Schiff base ligand (H_2L) was synthesized by adding dropwise dibenzoyl methane (17.83 mmol, 4 g) dissolved in acetone to an ethanolic solution of anthranilic acid (35.65 mmol, 4.89 g). The resulting mixture was magnetically stirred and refluxed for about 2 h during which a greenish yellow solid compound was precipitated. The ligand obtained was filtered, recrystallized, washed with acetone and dried in vacuum.

FT-IR (KBr, ν cm^{-1}): (O–H) 3372sh, (C=N) 1612sh, (C=O) 1671sh, $(COO)_{asym}$ 1558sh, $(COO)_{sym}$ 1419sh; ^1H NMR (300 MHz, DMSO, δ ppm): 12.98 (s, H, OH), 7.34–7.54 (m, 10H, Ar H benzoyl methane), 7.57–8.18 (m, 8H, Ar H amino benzoic acid), 4.87 (s, 2H, CH_2). The molecular ion peak was found at m/z = 461.78 amu, calcd: 462.00 amu. M.p.: 64 °C; yellow colour, percent yield: 90.0%. Anal. calcd for H_2L: C, 75.32; H, 4.70; N, 6.06., Found: C, 75.30; H, 4.50; N, 6.04.

Synthesis of metal complexes

A mixture of hot ethanolic solution (60 °C) of the metal chloride (8.65×10^{-4} mol) and the ligand (H_2L) (0.4 g, 8.65×10^{-4} mol) in a 1:1 molar ratio was prepared. The resulting mixture was stirred under reflux for 1 h whereupon the complexes were precipitated. After filtration and purification done by washing several times with hot ethanol, the metal complexes were collected.

$[Cr(L)(H_2O)_2]Cl$, Yield: (87%); Green colour; m.p: 100 °C; μ_{eff} (B.M) 4.10; Λ_m (Ω^{-1} mol^{-1} cm^2) 70.0; FT-IR (KBr, ν cm^{-1}): (OH) 3382br, (C=O) 1694w, (C=N) 1605w, $(COO)_{asym}$ 1533 s, $(COO)_{sym}$ 1407 s, H_2O (rocking and waging vibrations) 925w and 842w, (M–O, coordinated water) 520w, (M–O) 564w, (M–N) 431 m. Anal. Found: C, 59.36; H, 4.03; N, 4.56; Cr, 8.78; Calcd: C, 59.64; H, 4.11; N, 4.79; Cr, 8.91.

$[Mn(L)(H_2O)_2]$, Yield: (85%); Brown colour; m.p: 110 °C; μ_{eff} (B.M) 5.98; Λ_m (Ω^{-1} mol^{-1} cm^2) 8.0; FT-IR (KBr, ν cm^{-1}): (OH) 3472w, (C=O) 1668w, (C=N) 1591 m, $(COO)_{asym}$ 1543 s, $(COO)_{sym}$ 1458w, H_2O (rocking and waging vibrations) 925w and 853w, (M–O, coordinated water) 532w, (M–O) 556w, (M–N) 452w. Anal. Found: C, 63.09; H, 4.06; N, 5.05, Mn, 9.95; Calcd: C, 63.16; H, 4.35; N, 5.08; Mn, 9.90.

$[Fe(L)(H_2O)_2]Cl$, Yield: (80%); Brown colour; m.p: 118 °C; μ_{eff} (B.M) 5.08; Λ_m (Ω^{-1} mol^{-1} cm^2) 67.0; FT-IR (KBr, ν cm^{-1}): (OH) 3426br, (C=O) 1697 m, (C=N) 1591 m, $(COO)_{asym}$ 1526 s, $(COO)_{sym}$ 1480 s, H_2O (rocking and waging vibrations) 934w and 834w, (M–O, coordinated water) 543 m, (M–O) 564w, (M–N) 488 m. Anal. Found: C, 55.11; H, 3.14; N, 4.16, Fe, 9.08; Calcd: C, 55.21; H, 3.32; N, 4.43; Fe, 9.51.

$[Co(L)(H_2O)_2]$, Yield: (82%); Brown colour; m.p: 170 °C; μ_{eff} (B.M) 4.97; Λ_m (Ω^{-1} mol^{-1} cm^2) 35.0; FT-IR (KBr, ν cm^{-1}): (OH) 3402br, (C=O) 1689 m, (C=N) 1592 s, $(COO)_{asym}$ 1537 s, $(COO)_{sym}$ 1408 s, H_2O (rocking and waging vibrations) 950w and 869w, (M–O, coordinated water) 522w, (M–O) 562w, (M–N) 419 m. Anal. Found: C, 62.41; H, 4.17; N, 5.01, Co, 10.76; Calcd: C, 62.71; H, 4.32; N, 5.04; Co, 10.61.

$[Ni(L)(H_2O)_2]$, Yield: (87%); Green colour; m.p: ›300 °C; μ_{eff} (B.M) 3.44; Λ_m (Ω^{-1} mol^{-1} cm^2) 30.0; FT-IR (KBr, ν cm^{-1}): (OH) 3403br, (C=O) 1691 m, (C=N) 1594 s, $(COO)_{asym}$ 1540 s, $(COO)_{sym}$ 1406 s, H_2O (rocking and waging vibrations) 927w and 871w, (M–O, coordinated water) 520w, (M–O) 564w, (M–N) 494w. Anal. Found: C, 62.45; H, 4.23; N, 5.00, Ni, 10.55; Calcd: C, 62.73; H, 4.30; N, 5.04; Ni, 10.85.

$[Cu(L)(H_2O)_2]H_2O$, Yield: (80%); dark green colour; m.p: 110 °C; μ_{eff} (B.M) 1.68; Λ_m (Ω^{-1} mol^{-1} cm^2) 38.0; FT-IR (KBr, ν cm^{-1}): (OH) 3403br, (C=O) 1690 s, (C=N) 1594 s, $(COO)_{asym}$ 1525 m, $(COO)_{sym}$ 1455 m, H_2O (rocking and waging vibrations) 932w and 871w, (M–O, coordinated water) 545w, (M–O) 568 m, (M–N) 422 m. Anal. Found: C, 60.16; H, 4.36; N, 4.59, Cu, 10.98; Calcd: C, 60.25; H, 4.50; N, 4.84; Cu, 11.00.

$[Zn(L)(H_2O)_2]$, Yield: (86%); Brown colour; m.p: 184 °C; μ_{eff} (B.M) diamagnetic; Λ_m (Ω^{-1} mol^{-1} cm^2) 11.0; FT-IR (KBr, ν cm^{-1}): (OH) 3499br, (C=O) 1606 s, (C=N) 1560 s, $(COO)_{asym}$ 1508w, $(COO)_{sym}$ 1488 s, H_2O (rocking and waging vibrations) 926w and 850w, (M–O, coordinated water) 539w (M–O) 583w, (M–N) 468w. ^1H NMR (300 MHz, DMSO, δ ppm): disapear (s, H, OH), 6.46–7.51 (m, 10H, Ar H benzoyl methane), 7.54–8.17 (m, 8H, Ar H amino benzoic acid), 4.86 (s, 2H, CH_2). Anal. Found: C, 61.63; H, 4.01; N, 4.53, Zn, 11.34; Calcd: C, 61.98; H, 4.27; N, 4.98; Zn, 11.64.

$[Cd(L)(H_2O)_2]$, Yield: (83%); Brown colour; m.p: 220 °C; μ_{eff} (B.M) diamagnetic; Λ_m (Ω^{-1} mol^{-1} cm^2) 9.0; FT-IR (KBr, ν cm^{-1}): (OH) 3473 s, (C=O) 1671 s, (C=N) 1589 s, $(COO)_{asym}$ 1555 m, $(COO)_{sym}$ 1418 s, H_2O (rocking and waging vibrations) 917 m and 863w, (M–O,

coordinated water) 529w, (M–O) 566w, (M–N) 416w. ^{1}H NMR (300 MHz, DMSO, δ ppm): disappear (s, H, OH), 6.26–7.53 (m, 10H, Ar H benzoyl methane), 7.56–8.75 (m, 8H, Ar H amino benzoic acid), 4.87 (s, 2H, CH_2). Anal. Found: C, 57.02; H, 3.90; N, 4.35, Cd, 18.08; Calcd: C, 57.19; H, 3.94; N, 4.60; Cd, 18.47.

Biological activity

Antimicrobial activity

The biological activity test was carried out using diffusion agar technique [14–16]. The method was followed as previously described [15]. Four investigated bacteria (Gram positive bacteria: *Streptococcus pneumoniae* and *Bacillus Subtilis*; Gram negative bacteria: *Pseudomonas aeruginoa* and *Escherichia coli*) and fungi (*Aspergillus fumigatus*; *Syncephalastrum racemosum*; *Geotricum candidum* and *Candida albicans*) were used. By subtracting the diameter of inhibition zone resulting with DMSO from that obtained in each case, so antibacterial activity could be calculated [17, 18]. Amikacin and ketoconazole were used as reference compounds for antibacterial and antifungal activities, respectively. All experiments were performed as triplicate and data plotted were the mean value.

Anticancer activity

The cytotoxicity of the tested compounds was performed using the method of Skehan and Storeng [17] and the method followed as previously described [17]. Different concentrations of the compounds under investigation (0, 5, 12.5, 25, 50 and 100 µg/ml) were used and triplicate wells were prepared for each individual dose. The survival curve of breast tumor cell line for each compound was obtained through plotting the relation between surviving fraction and drug concentration and the percentage of cell survival was calculated as reported [17].

Results and Discussion

Characterization of the Schiff base ligand

The Schiff base ligand prepared by the reaction of anthranilic acid with dibenzoyl methane in a molar ratio 2:1. The ligand is yellow stable powder at room temperature. It is soluble in common organic solvents. The results of elemental analyses obtained are in good agreement with those calculated for the suggested formula of the ligand presented in the experimental part. The IR spectrum of H_2L ligand indicates the formation of the Schiff base due to the presence of newly appeared sharp strong vibration band at 1612 cm^{-1} attributed to the azomethine group ν(C=N) [19]. ^{1}H NMR spectrum has been used to ensure ligand structure and purity in *d6*-dimethylsulfoxide (DMSO-d_6) solution using Me_4Si (TMS) as internal standard [20]. The multiple in the region 7.34–8.18 ppm may be assigned to aromatic ring protons while the carboxylic acid group gives a sharp singlet at 12.98 ppm. The molecular ion peak appeared at (m/z) 461.78 amu in the mass spectrum of the H_2L ligand confirmed the proposed formula in which the ligand moiety is $C_{29}H_{22}N_2O_4$ with an atomic mass 462 amu. The proposed structure of the symmetric Schiff base ligand is given in Fig. 1.

Characterization of metal complexes

All the complexes are colored and stable to air and moisture. They are soluble in DMF. The complexes were characterized by different techniques such as elemental analyses, IR spectra, mass, ^{1}H NMR and thermal analyses.

Elemental analyses of complexes

Metal complexes have been synthesized by the reaction of the Schiff base dissolved in hot acetone with an ethanolic solution of the corresponding metal salt in a molar ratio 1:1. The experimental elemental analyses of complexes are in good compliance with the theoretical calculations. The elemental analyses of metal complexes (C, H, N and M) with molecular formula and the melting points are illustrated in the experimental part.

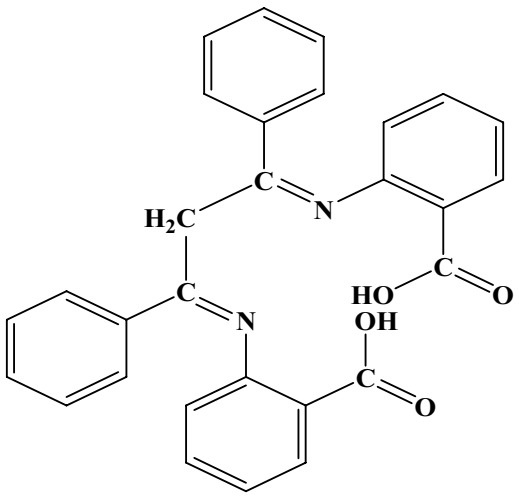

2,2'-((1Z,1'Z)-(1,3-diphenylpropane-1,3-diylidene) bis(azanylylidene))dibenzoic acid.

Fig. 1 Structure of the Schiff base ligand (H_2L)

Spectral studies

IR spectral studies The IR spectra of the complexes have been compared with those of the free ligand to determine the involvement of coordination sites in chelation. The data are listed in the experimental part. The IR spectrum of the ligand (H_2L) exhibits a band at 1612 cm^{-1} due to the azomethine ν(C=N) group [21, 22]. The band is shifted to lower frequencies in the spectra of the studied complexes (1548–1605 cm^{-1}) [23], indicating the participation of C=N in coordination to the metal ions [24]. A carbonyl ν(C=O) vibration band appears at 1671 cm^{-1} in the IR spectrum of the ligand is also shifted into lower or higher frequencies (1606–1697 cm^{-1}) in the complexes [25]. At 1558 cm^{-1} and 1419 cm^{-1} two strong bands referring to $\nu_{asym}(COO^-)$ and $\nu_{sym}(COO^-)$ vibrations of the free ligand are respectively observed [26]. The asymmetric carboxylate stretching $\nu_{asym}(COO^-)$ is shifted to (1480–1555 cm^{-1}) and the symmetric carboxylate stretching $\nu_{sym}(COO^-)$ is also shifted (1400–1488 cm^{-1}) in all complexes. These shifts indicate the linkage between the metal ions and carboxylate oxygen atom [27]. Broad bands are appeared in the 3382–3499 cm^{-1} range due to the stretching vibration of the ν(OH) of the carboxylic group in the spectra of the metal chelates while appeared at 3372 cm^{-1} in the spectrum of the Schiff base ligand [28]. Bands in the region 416–494 cm^{-1} and 556–583 cm^{-1} are assignable to ν(M–N) and ν(M–O) respectively, are also appeared in all complexes [20, 29]. Additionally, two bands at 917–950 and 834–871 cm^{-1} related to coordinated water molecules $\nu(H_2O)$ have been observed in the IR spectra of metal complexes, pointing the binding of water molecules to the metal ions [30]. New weak intensity bands belonging to (M–O) stretching vibrations have been noticed at 516–545 cm^{-1}. Accordingly, the ligand is acted as tetradendate chelating agent, and coordinates to the metal ion via two carboxylate oxygen and two azomethine nitrogen atoms. From the IR spectra we can conclude the formation of octahedral complexes through coordination by two water molecules in all complexes.

^{1}H NMR spectral studies of H_2L and its complexes The ^{1}H NMR spectra of the Schiff base ligand and its Zn(II) and Cd(II) complexes have been recorded in DMSO-d_6 by using tetramethylsilane (TMS) as internal standard. The chemical shifts of the different types of protons in the ^{1}H NMR spectra of the Schiff base and its complexes are listed in the experimental part. The aromatic ring protons of the ligand is predicted in the range of 7.34–7.54 ppm [31], while appear at 6.46–7.51 and 6.26–7.53 ppm in [Zn(L)$(H_2O)_2$] and [Cd(L)$(H_2O)_2$] complexes, respectively as shown in Figure S1 in the supplementary information. The COOH signal appears at 12.98 ppm in free Schiff base ligand, has been disappeared in [Zn(L)$(H_2O)_2$] and [Cd(L)$(H_2O)_2$] spectra. Referring to the data collected, we can illustrate that the ligand behaves as di-negative ligand which undergoes deprotonation during complexation process [32].

Mass analysis The mass spectra of the Cu(II) and Fe(III) complexes indicate the molecular ion peaks at m/z 576.77 and 586.58 amu, respectively. This results are consistent with the calculated weight 577.55 and 587.34 amu, respectively. These data confirmed the stoichiometry of these complexes as being of [ML] type.

Electronic spectral studies and magnetic susceptibility Electronic spectra of H_2L and its complexes were recorded at room temperature. The spectrum of H_2L (Figure S2) presents a band at 263 nm, which is assigned to $\pi \rightarrow \pi^*$ transitions of the aromatic rings. In addition, strong band has been also appeared at 342 nm which assigned to $n \rightarrow \pi^*$ transition of the azomethine group. Referring to the involvement of the azomethine group in coordination with metals, the bands were shifted to 253–346 nm for $\pi \rightarrow \pi^*$ transition and 341—537 nm for $n \rightarrow \pi^*$ transition in all complexes [33].

Three bands at 28,530, 25,252 and 19,157 cm^{-1} have been observed in the diffused reflectance spectrum of Cr(III) complex. These bands may be assigned to the $^4A_{2g}(F) \rightarrow {}^4T_{2g}(F)$, $^4A_{2g}(F) \rightarrow {}^4T_{1g}(F)$ and $^4A_{2g}(F) \rightarrow {}^4T_{2g}(P)$ spin allowed d-d transitions, respectively. Confirmation of the octahedral structure of Cr(III) complex has been also predicted from the magnetic moment value which is found to be 4.10 B.M. [34].

Manganese(II) complex exhibits four intensity absorption bands at 16,366, 22,371, 25,445 and 37,174 cm^{-1}, which may be assigned to the transitions: $^6A_{1g} \rightarrow {}^4T_{1g}$ (4G), $^4A_{1g}$(4G), $^6A_{1g} \rightarrow {}^4E_g$, $^6A_{1g} \rightarrow {}^4E_g$ (4D) (17B + 5C), $^6A_{1g} \rightarrow {}^4T_{1g}$ (4P), respectively [35]. The magnetic moment value is found to be 5.98 B.M; which indicates the presence of Mn(II) complex in octahedral structure [36].

From the diffused reflectance spectrum, Fe(III) chelate exhibits a band at 37,453 cm^{-1}, which may be assigned to the $^6A_{1g} \rightarrow T_{2g}(G)$ transition in the octahedral geometry of the complex [37]. The $^6A_{1g} \rightarrow {}^5T_{1g}$ transition splits into two bands at 26,666 cm^{-1} and 22,883 cm^{-1}. Another band at 47,846 cm^{-1}, is also appeared. This band may be attributed to ligand to metal charge transfer. The octahedral geometry of Fe(III) complex is also confirmed from the value of the observed magnetic moment which is 5.08 B.M.

Co(II) complex diffused reflectance spectrum, shows three bands in the 16,366, 17,376, and 21,008 cm^{-1} assigned to the $^4T_{1g})F(\rightarrow {}^4T_{2g})F($; $^4T_{1g})F(\rightarrow {}^4A_{2g})F($; and $^4T_{1g})F(\rightarrow {}^4T_{1g})P($ transitions, respectively, indicating the octahedral geometry around the Co(II) ion [36]. The observed magnetic moment value of 4.97 B.M. corresponds to high

spin state and further supports the octahedral geometry around Co(II) ion.

The diffused reflectance spectral data of Ni(II) complex reveal d-d bands in the region 16,694, 18.115 and 25,740 cm^{-1}, respectively [38], which may be assigned to $^3A_{2g}(F) \rightarrow {}^3T_{2g}(F)$, $^3A_{2g}(F) \rightarrow {}^3T_{1g}(F)$ and $^3A_{2g}(F) \rightarrow {}^3T_{2g}(F)$ transitions. These bands are distinctive to octahedral geometry of the Ni(II) complex [39]. The detected magnetic moment value of Ni(II) complex is 2.44 BM, this value is assigned to two unpaired electrons per Ni(II) ion. Having an octahedral geometry for nickel complex has been supported from data obtained [40].

Diffused reflectance spectrum of Cu(II) complex showed the d-d transition bands at 16,406, 19,569 and 26,809 cm^{-1} [41]. These bands correspond to $^2B_{1g} \rightarrow {}^2A_{1g}$ ($d_{x2-y2} \rightarrow d_{z2}$), $^2B_{1g} \rightarrow {}^2B_{2g}$ ($d_{x2-y2} \rightarrow d_{xy}$) and $^2B_{1g} \rightarrow {}^2E_g$ ($d_{x2-y2} \rightarrow d_{xz}$, d_{yz}) transitions, respectively. On the basis of electronic transitions, a distorted octahedral geometry is suggested for Cu(II) complex [39]. The obtained magnetic moment value of 2.68 BM for Cu(II) complex is indicative of one unpaired electron per Cu(II) ion for d^9-system suggesting spin-free distorted octahedral geometry [39]. Both of Zn(II) and Cd(II) complexes are diamagnetic. An octahedral geometry is proposed for these chelates according to their suggested empirical formulae.

Electron spin resonance spectrum of Cu(II) complex The ESR spectrum of Cu(II) complex has been studied and presented in Fig. 2. The spectrum consisted of two signals, one with four hyperfine-structure lines at low magnetic field (the $g_{\parallel}$ signal) and the other at high field ($g_{\perp}$ signal) [41]. The trend $g_{\parallel} > g_{\perp} >$ free electron-spin (2.0023), indicates that the unpaired electron is localized in d_{x2-y2} orbital of the Cu(II) ion [42] and the spectral figure is characteristic for distorted octahedral sites (D_{4h}) [43]. The spectrum of $[Cu(L)(H_2O)_2]H_2O$ complex exhibits a broad $g_{\perp}$ component, with splitting of $g_{\parallel}$ component, reflects the coupling with the Cu(II) nucleus (I = 3/2). The reported parameters showed the $g_{\parallel}$ value at 2.12 and $g_{\perp}$ at 1.96 [44]. The $g_{\parallel}$ value in a copper(II) complex can be used as a measure of the covalent character of the metal–ligand bond [44]. Knowing that if the value of $g_{\parallel}$ is more than 2.3 the environment is essentially ionic. While a covalent environment is indicated if the value of $g_{\parallel}$ is less than 2.3. The $g_{\parallel}$ value interpreted for Cu(II) complex reveals considerable mixed ionic-covalent bonding character [45]. Referring to Hathaway [46], the parameter G, calculated by the given relation as $G = (g_{\parallel} - 2) / (g_{\perp} - 2)$. If G is greater than 4, the exchange interaction may be negligible; however, if G is less than 4, a considerable exchange interaction will be considered as indication in the solid complex [47, 48]. The value of calculated G parameter for the Cu(II) complex is 3.2, indicating a considerable exchange interaction between the copper centers in the solid [48].

Molar conductivity measurements

All metal complexes are non-electrolytes except Cr(III) and Fe(III) complexes have molar conductance values of 70 and 67 Ω^{-1} mol^{-1} cm^2, respectively, proving the ionic nature of these complexes. The measured molar conductivity values of 10^{-3} M metal complexes in DMF at 25 °C are reported in the experimental part.

Thermal analysis studies (TG and DTG)

The thermal studies of ligand and its metal complexes were carried out using the thermogravimetric technique (TG) and differential thermogravimetric (DTG) analyses. The thermal analysis gives useful data for the thermal stability of the

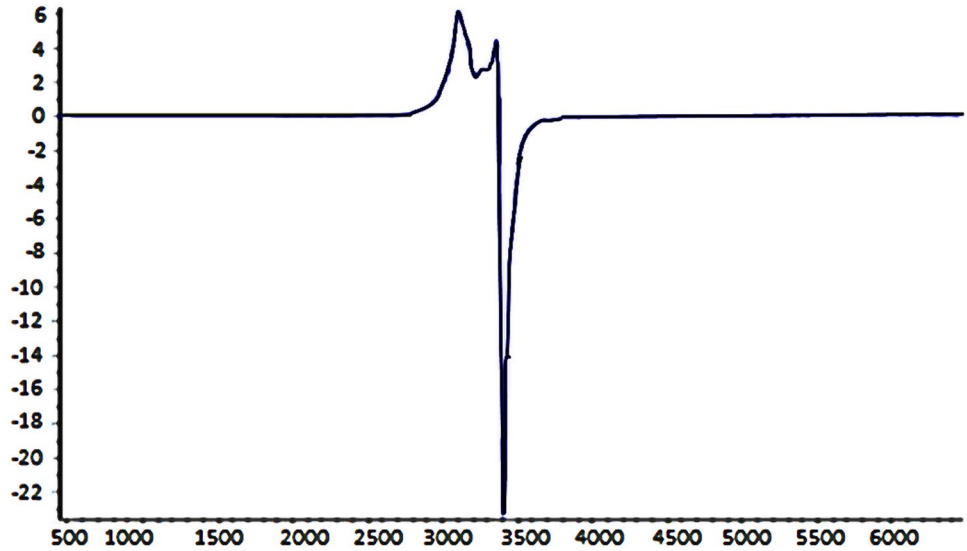

Fig. 2 ESR spectrum of $[Cu(L)(H_2O)_2]H_2O$ complex

Table 1 Thermoanalytical results (TG and DTG) of H_2L ligand and its metal complexes

Complex	TG range (°C)	DTG_{max} (°C)	n*	Mass loss Estim (Calcd) %	Total mass loss	Assignment	Residues
H_2L	152–367	182, 352	2	99.92 (98.71)	99.92 (98.71)	- Loss of $C_{29}H_{22}N_2O_4$	–
$[Cr(L)(H_2O)_2]Cl$	130–250	150, 222	2	36.54 (37.27)	79.93 (80.80)	-Loss of $2H_2O$, HCl, CO_2 and C_7H_3N	$3C + ½\ Cr_2O_3$
	250–470	415	1	43.38 (43.53)		-Loss of $C_{18}H_{16}NO_{0.5}$	
$[Mn(L)(H_2O)]$	150–500	189, 453	2	80.19 (80.58)	80.19 (80.58)	- Loss of $2H_2O$, CO_2 and $C_{25}H_{20}N_2O$	2C + MnO
$[Fe(L)(H_2O)_2]Cl$	120–230	169	1	35.25 (34.98)	81.85 (82.07)	- Loss of $2H_2O$, HCl, CO_2 and C_6H_3N	$3C + ½\ Fe_2O_3$
	230 – 586	401, 557	2	45.18 (45.28)		- Loss of $C_{19}H_{16}NO_{0.5}$	
$[Co(L)(H_2O)_2]$	140–205	173	1	46.86 (46.67)	78.41 (78.20)	- Loss of $2H_2O$, CO_2 and $C_{13}H_9N$	4C + CoO
	205–432	392	1	31.55 (31.53)		- Loss of CO and $C_{10}H_{13}N$	
$[Ni(L)(H_2O)_2]$	140–265	172	1	49.32 (49.21)	80.72 (80.03)	- Loss of $2H_2O$, CO_2 and $C_{14}H_{11}N$	3C + NiO
	265–425	400	1	31.40 (30.82)		- Loss of $C_{11}H_9NO$	
$[Cu(L)(H_2O)_2]H_2O$	60–115	89	1	3.22 (3.11)	77.83 (77.90)	- Loss of H_2O	4C + CuO
	115–345	168, 304	2	74.61 (74.79)		- Loss of $2H_2O$, CO_2 and $C_{24}H_{20}N_2O$	
$[Zn(L)(H_2O)_2]$	170–210	190	1	45.71 (46.13)	76.10 (76.94)	- Loss of $2H_2O$, CO_2 and $C_{13}H_9N$	4C + ZnO
	210–650	352, 623	2	30.38 (30.81)		- Loss of CO and $C_{10}H_{11}N$	
$[Cd(L)(H_2O)_2]$	150–240	195	1	76.52 (76.92)	76.52 (76.92)	- Loss of $2H_2O$, CO_2 and $C_{27}H_{20}N_2O$	C + CdO

n* = number of decomposition steps

metal complexes. The TG and DTG was recorded within the temperature range from 30 to 1000 °C (Table 1).

The Schiff base ligand (H_2L) with the molecular formula ($C_{29}H_{22}N_2O_4$) was thermally decomposed in two successive decomposition steps. The first and second steps with an estimated mass loss of 99.92% (calculated mass loss = 98.71%) within the temperature range 152–367 °C may be attributed to the loss of $C_{29}H_{22}N_2O_4$ molecule. The DTG curve gives two maximum peaks temperature at 182–352 °C. The overall weight loss amounts to 99.92% (calculated mass loss = 98.71%).

Three decomposition steps have been recorded in the thermogravimetric (TG) curve for $[Cr(L)(H_2O)_2]Cl$ complex. The two steps of decomposition occurred within the range of 134–250 °C, with two maxima at 150 and 222 °C. They are related to the loss of two coordinated H_2O, HCl molecule, CO_2 gas and C_7H_3N fragment with an estimated mass loss of 36.54% (calculated mass loss = 37.27%). The third step takes place in the range of 385–470 °C which corresponds to loss of $C_{18}H_{16}NO_{0.5}$ fragment with appraisal mass loss of 43.38% (calculated mass loss = 43.53%) leaving $½Cr_2O_3$ mixed with carbon as final precipitate product. The total weight loss found is 79.93% (calculated mass loss = 80.80%).

The decomposition procedure resulted from the TG curve of $[Mn(L)(H_2O)_2]$ complex shows two steps. The first and second steps have been occurred in the range of 152–499 °C with two maximum temperatures at 189 and 453 °C which illustrate the loss of $2H_2O$, CO_2 gas and $C_{25}H_{20}N_2O$ fragment with an appraisal weight loss 80.19%, however the calculated mass loss is 80.58%. The rest of the complex has been found as MnO contaminated with carbon.

Thermogravimetric (TG) curve for $[Fe(L)(H_2O)_2]Cl$ chelate displayed three weight loss stages. The first stage happened in the range of 121–232 °C with maximum temperature at 169 °C which referred to the loss of the two coordinated water molecules, CO_2 gas, HCl molecule and C_6H_3N fragment with proposed mass loss of 35.25%, while the calculated mass loss is 34.98%. The second and third stages recorded within the temperature range from 366 °C to 586 °C with two maxima temperatures at 401 °C and 557 °C which may be correlated to the loss of $C_{19}H_{16}NO_{0.5}$ fragment with estimated mass loss 45.18%, knowing that the calculated mass loss is 45.28%. The residue is $½Fe_2O_3$ contaminated with carbon. The total weight loss is found to be 80.43% (calculated mass loss = 80.26%).

$[Co(L)(H_2O)_2]$ complex was thermally decomposed in two stages. The first step is derived within a temperature range from 144 °C to 208 °C with maximum temperature 173 °C. This step could be correlated to the escaping of two H_2O molecules, CO_2 gas and $C_{13}H_9N$ part (Found/calcd. = 46.86%/ 46.67%). The second decomposition step has been occurred in the temperature range from 360 to 432 °C with one maximum at 392 °C. The estimated mass loss of 31.55% (calculated mass loss = 31.53%). We can refer this step to the complete decomposition of CO in addition to a decomposition of $C_{10}H_{13}N$ molecule as part of ligand. CoO contaminated with carbon is rest as final product. The overall weight loss amounted to 78.41% (calcd. 78.20%).

The TG curve of $[Ni(L)(H_2O)_2]$ complex reveals decomposition from 144 °C to 425 °C in two stages. First stage observed within the temperature range of 144–265 °C with maximum temperature at 172 °C which related to the elimination of $2H_2O$ molecules, CO_2 gas and $C_{14}H_{11}N$ molecule as a fragment. The mass loss (found/ calcd.:49.32%/49.21%). The second stage represents the loss of CO gas and $C_{10}H_9N$ molecule with a mass loss of 31.40% (calcd. = 30.82%) and the temperature ranged from 366 °C to 425 °C with maxima at 400 °C. The metal oxide NiO contaminated with carbons is the residue with total estimated mass loss of 80.72% (calcd. = 80.03%).

$[Cu(L)(H_2O)_2]H_2O$ chelate has been thermally decomposed in three steps within the temperature range from 66 to 346 °C. The first decomposition step with an estimated mass loss of 3.22% (calcd. = 3.11%) has been occurred within the temperature range from 66 to 115 °C with maximum temperature at 89 °C. The second and third decomposition steps have been occurred within the range of 135–346 °C with two maximum temperatures at 168 and 304 °C. These steps may be attributed to elimination of $2H_2O$ coordinated water and CO_2 gas and $C_{24}H_{20}N_2O$ fragment. CuO contaminated with carbon is the residue. The overall weight loss (found/ calcd.77.83%/77.90%).

The $[Zn(L)(H_2O)_2]$ chelate is decomposed in three steps. The first step has been happened by giving off two coordinated water molecules, CO_2 gas and $(C_{13}H_9N)$ molecule within the temperature range of 172–211 °C with maximum temperature at 190 °C. The found mass loss of 45.71% while the calculated mass loss is 46.13%. In the next two steps the complex loss CO gas and $C_{10}H_{11}N$ fragment within the temperature range of 341–651 °C and with two maxima temperature at 352 and 623 °C. The estimated mass loss is (found/calcd.:30.38%/30.81%). ZnO contaminated with carbons is the final product with total approximated mass loss (found/calcd. 76.10%/76.94%).

$[Cd(L)(H_2O)_2]$ complex was thermally decomposed in one step within the temperature range from 155 to 239 °C with maximum temperature at 195 °C. In this step, two coordinated water molecules, CO_2 gas and $C_{27}H_{20}N_2O$ ligand molecule were evolved. The estimated mass loss of 76.52% (calcd. = 76.92%). CdO contaminated with carbon is the final residue.

Structural interpretation

The suggested structures of metal complexes resulted from the reaction of the Schiff base ligand (H_2L) with the studied metal ions were identified from the study of elemental analyses, molar conductivity, magnetic, solid reflectance and thermal analysis data. From IR spectra, it could be concluded that H_2L behaves as a di-negatively tetradentate ligand coordinated to the metal ions via two nitrogen atoms of azomethine group and two oxygen atoms of carboxylate group. The complexes were found to be non-electrolytes expect Cr(III) and Fe(III) complexes, depending on the results obtained from the molar conductivity study. The structure of metal complexes is given in Fig. 3.

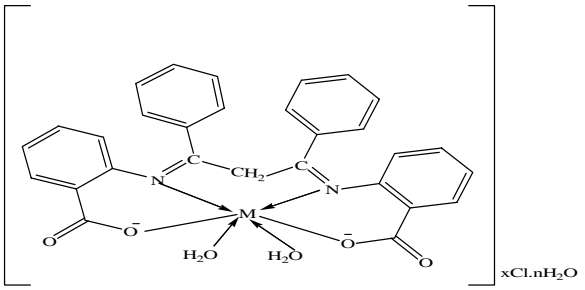

Fig. 3 Structure of metal complexes of Schiff base ligand (H_2L)

Biological activity

Referring on Overtone's concept and Tweedy's chelation theory [49], the biological activity of metal complexes has been explained. As the metal complex has high activity rather than the free ligand regarding the greater lipophilic nature of the complex. According to Overtone's concept of cell permeability, the lipid membrane that surrounds the cell prefers the passage of only lipid soluble materials due to which liposolubility is deemed to be an important reason that rules the antimicrobial activity. On complexation, the polarity of the metal ion will be decreased to a greater extent due to the overlap of the ligand orbital and partial sharing of positive charge of metal ion with donor groups. Moreover, it increases the delocalization of the π electrons over the whole chelate ring and boost the lipophilicity of the chelate. The increases in lipophilicity will enhance the permeation of the chelates into lipid membrane and thus blocked the metal binding sites on enzymes of microorganisms. The chelates also disturb the respiration process of the cell and thus block the synthesis of proteins, which tighten the growth of the microorganism. Factors such as solubility, conductivity and bond length between the metal ion and ligand are also taken in consideration to explain the increases in activity [50–52].

Antimicrobial activity in vitro using four fungi species (*A. fumigatus; S.yracemosum; G. candidum* and *C. albicans*) and two Gram-negative bacteria (*P. aeruginosa* and *E. coli*) and two Gram-positive bacteria (*S. pneumoniae* and *B. Subtilis*) were evaluated against Schiff base and its metal complexes [53].

Measurement of the zone of inhibition diameters of the tested organisms against the ligand (H_2L) and its metal

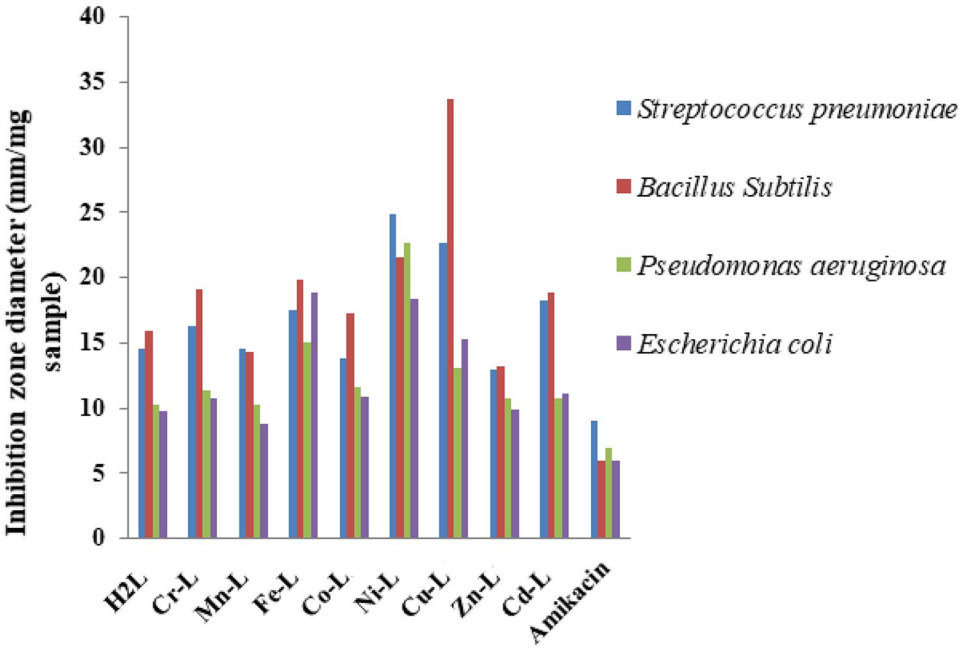

Fig. 4 Biological activity of Schiff base ligand (H_2L) and its metal complexes with Gram positive and Gram negative organisms

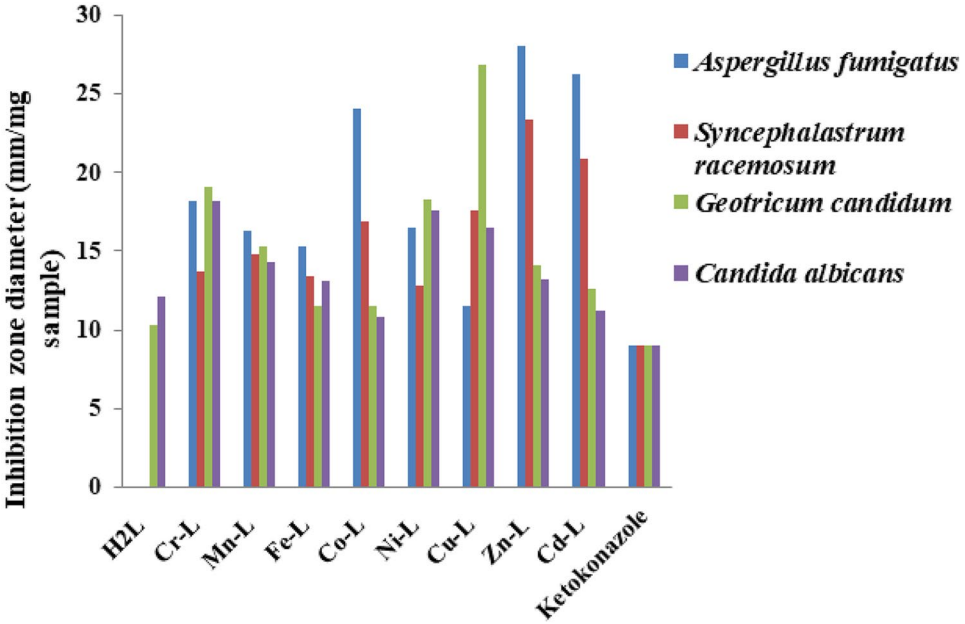

Fig. 5 Biological activity of Schiff base ligand (H_2L) and its metal complexes with fungi

complexes is presented in Figs. 4 and 5 and Tables 2 and 3. DMSO was included as a negative control while amikacin and ketoconozole drugs were included as positive standards for antibacterial and antifungal studies, respectively [30].

Ni(II), Cu(II), Cd(II), Fe(III) and Cr(III) complexes show significant activity than the free H_2L ligand against *S. pneumoniae* as G + bacteria. While Mn(II) complex has the same biological activity of free H_2L ligand. The biological activity of the Co(II) and Zn(II) complexes are low comparing to the free ligand. Using *B. Subtilis* as G + bacteria, the biological activity of Cu(II), Ni(II), Fe(III), Cr(III), Cd(II) and Co(II) complexes show higher activity than that of the free H_2L ligand. In contrary, the biological activity of the Mn(II) and Zn(II) complexes is found to be lower than free H_2L ligand. The effect of Ni(II), Fe(III), Cu(II), Co(II) and Cr(III) complexes on G− bacteria *P. aeruginosa,* revealed significant activity in comparison to that obtained from the free H_2L ligand. While Cd(II), Zn(II) and Mn(II) complexes show equal activity as that of free H_2L ligand. Using *E. coli* as G− bacteria, the biological activity of Fe(III), Ni(II), Cu(II), Cd(II), Co(II) and Cr(III) complexes are high relative to that of the free

Table 2 Biological activity of Schiff base ligand (H_2L) and its metal complexes with Gram-positive bacteria and Gram-negative bacteria

Sample	Inhibition zone diameter (mm / mg sample)			
	(Gram- positive)		(Gram- negative)	
	Streptococcus pneumoniae	*Bacillus Subtilis*	*Pseudomonas aeruginosa*	*Escherichia coli*
Control: DMSO	0	0	0	0
H_2L	14.6 ± 0.42	15.9 ± 0.53	10.2 ± 0.21	9.8 ± 0.31
$[Cr(L)(H_2O)_2]Cl$	16.3 ± 0.42	19.1 ± 0.51	11.4 ± 0.36	10.7 ± 0.31
$[Mn(L)(H_2O)_2]$	14.6 ± 0.58	14.3 ± 0.58	10.2 ± 0.31	8.8 ± 0.24
$[Fe(L)(H_2O)_2]Cl$	17.5 ± 0.44	19.8 ± 0.63	15.1 ± 0.45	18.9 ± 0.25
$[Co(L)(H_2O)_2]$	13.8 ± 0.40	17.2 ± 0.43	11.6 ± 0.36	10.9 ± 0.21
$[Ni(L)(H_2O)_2]$	24.9 ± 0.63	21.5 ± 0.34	22.7 ± 0.56	18.4 ± 0.41
$[Cu(L)(H_2O)_2]H_2O$	22.6 ± 0.34	33.7 ± 0.25	13.1 ± 0.32	15.3 ± 0.48
$[Zn(L)(H_2O)_2]$	12.9 ± 0.63	13.2 ± 0.58	10.7 ± 0.24	9.9 ± 0.34
$[Cd(L)(H_2O)_2]$	18.2 ± 0.68	18.9 ± 0.64	10.8 ± 0.41	11.1 ± 0.43
Amikacin	9	6	7	6

Table 3 Biological activity of Schiff base ligand (H_2L) and its metal complexes with fungi

Sample	Inhibition zone diameter (mm/mg sample)			
	(*fungi*)			
	Aspergillus Fumigatus	*Syncephalastrum racemosum*	*Geotricum candidum*	*Candida albicans*
Control: DMSO	0	0	0	0
H_2L	0	0	10.3 ± 0.19	12.1 ± 0.26
$[Cr(L)(H_2O)_2]Cl$	18.2 ± 0.56	13.7 ± 0.39	19.1 ± 0.45	18.2 ± 0.44
$[Mn(L)(H_2O)_2]$	16.3 ± 0.35	14.8 ± 0.46	15.3 ± 0.52	14.3 ± 0.58
$[Fe(L)(H_2O)_2]Cl$	15.3 ± 0.55	13.4 ± 0.35	11.5 ± 0.58	13.1 ± 0.3
$[Co(L)(H_2O)_2]$	24.1 ± 0.51	16.9 ± 0.52	11.5 ± 0.43	10.8 ± 0.46
$[Ni(L)(H_2O)_2]$	16.5 ± 0.58	12.8 ± 0.27	18.3 ± 0.56	17.6 ± 0.54
$[Cu(L)(H_2O)_2]H_2O$	11.5 ± 0.58	17.6 ± 0.27	26.9 ± 0.35	16.5 ± 0.5
$[Zn(L)(H_2O)_2]$	28.1 ± 0.76	23.4 ± 0.77	14.1 ± 0.65	13.2 ± 0.58
$[Cd(L)(H_2O)_2]$	26.3 ± 0.73	20.9 ± 0.61	12.6 ± 0.54	11.2 ± 0.44
Ketokonazole	9	9	9	9

H_2L ligand. For Zn(II) complex, its biological activity is the same like the free H_2L ligand. While the Mn(II) complex has lower biological activity than that of the free H_2L ligand.

The antifungal studies showed, by using *C. albicans fungus*, that Cr(III), Ni(II), Cu(II), Mn(II), Zn(II) and Fe(III) complexes perform higher activity than that of the free H_2L ligand. The comparative study also revealed the lower biological activity of Cd(II) and Co(II) complexes than that of the free H_2L ligand. For *G. candidum fungus*, the effect of all metal complexes is higher than that of the free H_2L ligand. Differences in activity has been recorded for Cu(II) complex as the highest active complex and for Co(II) and Fe(III) as the lowest active. With *S. racemosum fungus,* no antifungal activity of the free H_2L ligand has been found. However, Zn(II) and Ni(II) complexes recorded the highest and lowest activity, respectively. Using *A. fumigatus fungus,* the highest biological activity is observed for the Zn(II) complex but Cu(II) complex shows the lowest activity. However, no significant activity has been observed for the free H_2L ligand.

Calculated activity index according to the relation below for the prepared Schiff base ligand and its metal complexes confirm their activity [54–56]:

$$\text{Activity index (A)} = \frac{\text{Inhibition zone of compound(mm)} \times 100}{\text{Inhibition zone of standard drug (mm)}}$$

From the data collected, Cu(II) complex was found to have the highest activity index [57], while Fe(III) complex has the lowest activity index as shown in Fig. 6 [42].

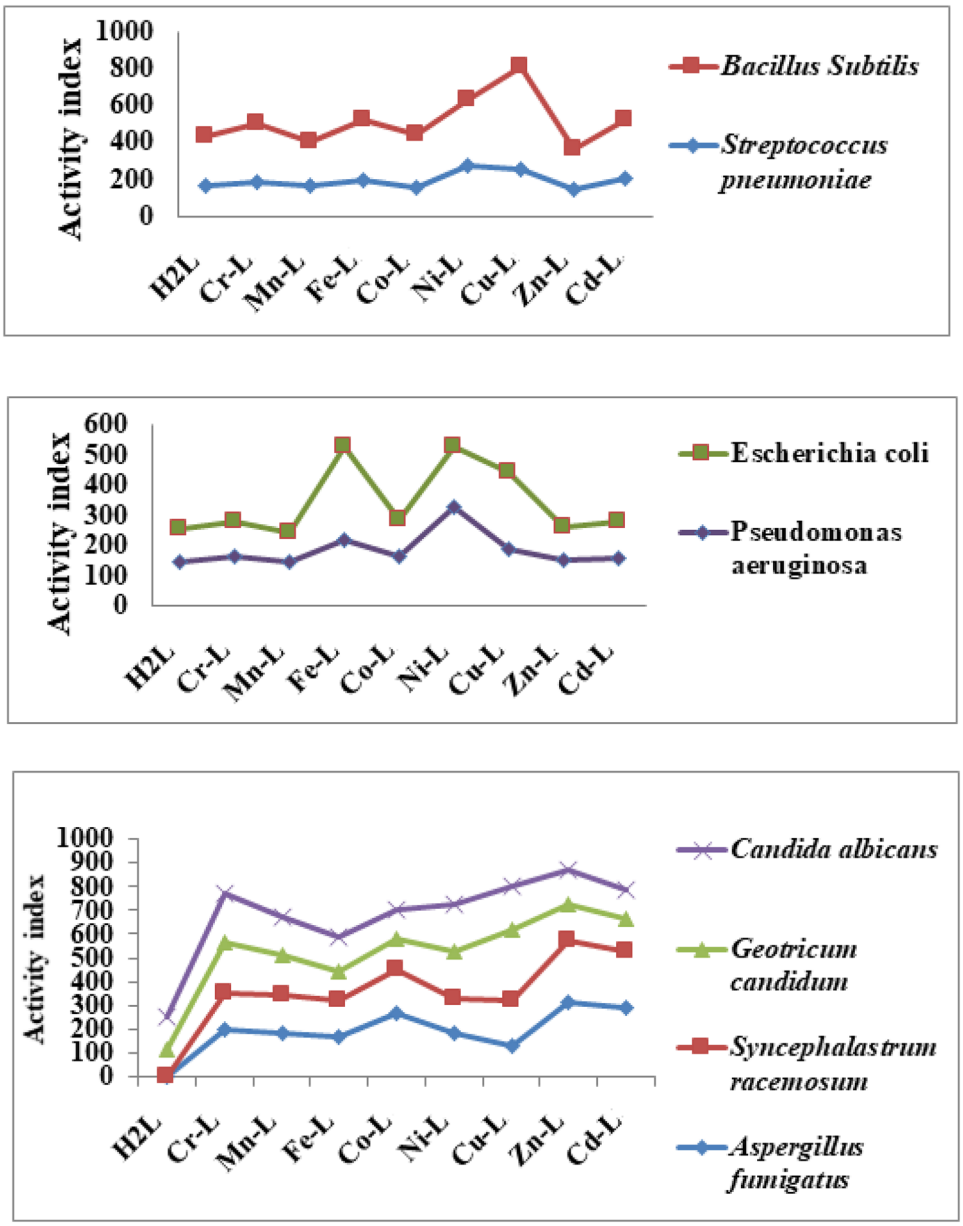

Fig. 6 Activity index value of Schiff base ligand (H_2L) and its metal complexes

Anticancer activity evaluation

Anticancer activity of the ligand and its complexes against human breast cancer cell line MCF 7 was traced. No inhibitory activity has been recorded as the range of inhibition of cell growth of ligand and its complexes is between 33 and 56%. As the results of inhibition of cell growth is lower than 70%, taking further testing with different concentration was not feasible.

Conclusion

Schiff base ligand 2,2′-((1Z-1′Z)-(1,3-diphenylpropane-1,3diylidene) bis (azanylyli- dene)) dibenzoic acid (H_2L) and its bi/trivalent transition metal complexes have been prepared and characterized. The ligand acts as binegative tetradentate through two azomethine nitrogens and two carboxylate oxygens and all complexes show octahedral geometry. All complexes are non-electrolyte expect Fe(III) and Cr(III) complexes are electrolytes, with the type of 1:1 electrolyte. The complexes general formulae $[M(L)(H_2O)_2]$ (M = Mn(II), Cu(II), Ni(II), Co(II), Zn(II) and Cd(II));$[M(L)(H_2O)_2]Cl$ (M = Cr(III) and Fe(III)). From the biological activity results, some complexes are higher

than free ligand. The Cu(II) complex has the highest activity index, while Fe(III) complex has the lowest activity index. Neither the free ligand, nor the complexes show anticancer activity.

Supplementary Information The online version contains supplementary material available at https://doi.org/10.1007/s13738-023-02868-w.

Funding Open access funding provided by The Science, Technology & Innovation Funding Authority (STDF) in cooperation with The Egyptian Knowledge Bank (EKB).

References

1. P. Przybylski, A. Huczynski, K. Pyta, B. Brzezinski, F. Bartl, Curr. Org. Chem. **13**, 124 (2009)
2. S. Malik, S. Ghosh, L. Mitu, J. Serb. Chem. Soc. **76**, 1387 (2011)
3. N. Raman, S. Raja, J. Joseph, J. Raja, J. Chil. Chem. Soc. **52**, 1138 (2007)
4. M. Alias, H. Kassum, C. Shakir, J. Assoc. Arab Univ. Basic Appl. Sci. **15**, 28 (2014)
5. P. Subbaraj, A. Ramu, N. Raman, J. Dharmaraja, J. Saudi Chem. Soc. **19**, 207 (2015)
6. D.C. Ware, H.R. Palmer, P.J. Brothers, C.E.F. Rickard, W.R. Wilson, W.A. Denny, J. Inorg Bichem. **68**, 215 (1997)
7. V.K. Srivastava, Future. J. Pharm. Sci. **7**, 1 (2021)
8. A. Sahraei, H. Kargar, M. Hakimi, M.N. Tahir, Transit Met. Chem. **42**, 483 (2017)
9. A. Sahraei, H. Kargar, M. Hakimi, M.N. Tahir, J. Mol. Struct. **1149**, 576 (2017)
10. A.A. Ardakani, H. Kargar, N. Feizi, M.N. Tahir, J. Iran. Chem. Soc. **15**, 1495 (2018)
11. H. Kargar, A.A. Ardakani, M.N. Ashhaq, K.S. Munawar, J. Mol. Struct. **1229**, 129842 (2021)
12. H. Kargar, F.A. Meybodi, R. Ardakani, M.R. Elahifard, K. Munawar. J. Mol. Struct. **1230**, 129908 (2021)
13. H. Kargar, J. Iran. Chem. Soc. (2021). https://doi.org/10.1007/s13738-021-02207-x
14. M.A. Pfaller, L. Burmeister, M.S. Bartlett, M.G. Rinaldi, J. Clin. Microbiol. **26**, 1437 (1988)
15. National Committee for Clinical Laboratory Standards, *Performance standards for antimicrobial susceptibility testing: twelfth informational supplement, M100–S12* (NCCLS, Wayne, PA, USA, 2002)
16. National committee for clinical laboratory standards methods for dilution antimicrobial susceptibility tests for bacteria that grow aerobically, *Approved Standard M7–A6*, 6th edn. (NCCLS, Wayne, PA, 2003)
17. P. Skehan, R. Storeng, D. Scudiero, A. Monks, J. McMahon, D. Vistica, J.T. Warren, H. Bokesch, S. Kenney, M.R. Boyd, J. Natl. Cancer Ins. **82**, 1107 (1990)
18. I. Sakıyan, E. Loğoğlu, S. Arslan, N. Sari, N. Şakıyan, Biometals **17**, 115 (2004)
19. M.A. Mahmoud, S.A. Zaitone, A.M. Ammar, S.A. Sallam, J. Mol. Struct **1108**, 60 (2016)
20. G. Kumar, S. Devi, D. Kumar, J. Mol. Struct. **1108**, 680 (2016)
21. Z. Guo, R. Xing, S. Liu, H. Yu, P. Wang, C. Li, P. Li, Bioorganic Med. Chem. Lett. **15**, 4600 (2005)
22. K. Poonia, S. Siddiqui, M. Arshad, D. Kumar, Spectrochim. Acta Part A Mol. Biomol. Spectrosc. **155**, 146 (2016)
23. P.A. Ajibade, G.A. Kolawole, P. O'Brien, M. Helliwell, J. Raftery, Inorganica Chim. Acta **359**, 3111 (2006)
24. N. Mahalakshmi, R. Rajavel, Arab. J. Chem. **7**, 509 (2014)
25. L.J. Li, B. Fu, Y. Qiao, C. Wang, Y.Y. Huang, C.C. Liu, C. Tian, J.L. Du, J. Inorganica Chim. Acta **419**, 135 (2014)
26. R. Gnanasambandam, A. Proctor, J. Food Chem. **68**, 327 (2000)
27. M.S. Nair, R.S. Joseyphus, Spectrochim. Acta Part A Mol. Biomol. Spectrosc. **70**, 749 (2008)
28. T.T. Liu, Y.W. Tseng, T.S. Yang, J. Food Chem. **190**, 1102 (2016)
29. A.Z. El-Sonbati, M.A. Diab, A.A. El-Bindary, G.G. Mohamed, Sh.M. Morgan, M.I. Abou-Dobara, S.G. Nozha, J. Mol. Liq. **215**, 423 (2016)
30. H.F. Abd El-Halim, F.A. Nour El-Dien, G.G. Mohamed, N.A. Mohamed, J. Therm. Anal. Calorim. **109**, 883 (2012)
31. S. Chithiraikumar, M.A. Neelakantan, J. Mol. Struct **1108**, 654 (2016)
32. E.M. Zayed, E.H. Ismail, G.G. Mohamed, M.M.H. Khalil, A.B. Kamel, J. Monatsh. Chem. **145**, 755 (2014)
33. S. Shit, A. Sasmal, P. Dhal, C. Rizzoli, S. Mitra, J. Mol. Struct. **1108**, 475 (2016)
34. W.H. Mahmoud, G.G. Mohamed, M.M.I. El-Dessouky, J. Mol. Struct. **1082**, 12 (2015)
35. R. Kumar, S. Chandra, Spectrochim. Acta Part A Mol. Biomol. Spectrosc. **67**, 188 (2007)
36. N.A. Mangalam, S.R. Sheeja, M.R.P. Kurup, J. Polyhedron **29**, 3318 (2010)
37. F.A. Cotton, G. Wilkinson, C.A. Murillo, M. Bochmann, *Advanced Inorganic Chemistry*, 6th edn. (Wiley, New York, 1999)
38. H.F. Abd El-Halim, G.G. Mohamed, Appl. Organometal. Chem. **32**, 4176 (2018)
39. P. Tyagi, S. Chandra, B.S. Saraswat, D. Sharma, Spectrochim. Acta Part A Mol. Biomol. Spectrosc. **143**, 1 (2015)
40. S. Chandraa, K. Ruchi, S. Qanungo, K. Sharma, Spectrochim. Acta Part A Mol. Biomol. Spectrosc. **79**, 1326 (2011)
41. M. Tyagi, M. Kumari, R. Chatterjee, A.C. Sun, P. Sharma, J. IEEE Trans. Magn. **50**, 2500704 (2014)
42. H.F. AbdEl-Halim, G.G. Mohamed, E. Khalil, J. Mol. Struct. **1146**, 153 (2017)
43. N. Raman, S.J. Raja, J. Serb. Chem. Soc. **72**, 983 (2007)
44. S. Chandra, Spectrochim. Acta Part A Mol. Biomol. Spectrosc. **129**, 333 (2014)
45. D. Kivelson, R. Neiman, J. Chem. Phys. **35**, 149 (1961)
46. B.J. Hathaway, D.E. Billing, J. Coord. Chem. Rev. **5**, 143 (1970)
47. X. Wang, J. Ding, J.D. Ranford, J.J. Vittal, J. Appl. Phys. **93**, 7819 (2003)
48. N. Aiswarya, M. Sithambaresan, S.S. Sreejith, S.W. Ng, M.R.P. Kurup, J. Inorganica Chim. Acta **443**, 251 (2016)
49. B.G. Tweedy, Phytopathology **55**, 910 (1964)
50. Z.H. Chohan, A. Munawar, C.T. Supuran, J. Met-Based Drugs **8**, 137 (2001)
51. J. Iqbal, S.A. Tirmizi, F.H. Wattoo, M. Imran, M.H.S. Wattoo, S. Sharfuddin, S. Latif, Turk. J. Biol. **30**, 1 (2006)
52. V.P. Singh, A. Katiyar, S. Singh, J. BioMetals **21**, 491 (2008)

53. A. Soroceanu, L. Vacareanu, N. Vornicu, M. Cazacu, V. Rudic, T. Croitori, J. Inorganica Chim. Acta **442**, 119 (2016)
54. H.F. AbdEl- Halim, M.M. Omar, G.G. Mohamed, M.A. Sayed, Eur. J. Chem. **2**, 178 (2011)
55. S. Gopalakrishnan, R. Rajameena, E. Vadivel, Int. J. Pharm. Sci. Res. **4**, 31 (2012)
56. E. Ramachandran, V. Gandin, R. Bertani, P. Sgarbossa et al., Molecules **25**, 25081868 (2020)
57. H. Kargar, F.A. Meybodi, M. Elahifard, M. Tahir, M. Ashfaq, K. Munawar, J. Coord. Chem. **74**, 1534 (2021)